Nuclear resonance fluorescence of ^{237}Np

C. T. Angell,* R. Yee, T. H. Joshi, E. Swanberg, and E. B. Norman†
Department of Nuclear Engineering, University of California, Berkeley, California 94720, USA

C. L. Hicks Jr., A. Klimenko,‡ S. Korbly, and C. Wilson
Passport Systems Inc., Billerica, Massachusetts 01862, USA

W. D. Kulp
Department of Physics, Georgia Institute of Technology, Atlanta, Georgia 30332, USA

G. A. Warren
Pacific Northwest National Laboratory, Richland, Washington 99352, USA

T. H. Bray, R. Copping, P. A. Glans, T. Tyliszczak, and D. K. Shuh
Chemical Sciences Division, Lawrence Berkeley National Laboratory, Berkeley, Caifornia 94720, USA
(Received 20 July 2010; published 15 November 2010)

Measurements of states excited by nuclear resonance fluorescence in ^{237}Np were performed using a bremsstrahlung beam. Fifteen new states were observed in the region of 1.7 to 2.5 MeV. They can be used to detect or assay ^{237}Np nondestructively for applications in security and safeguards. The states are populated with similar strength as those states found previously in ^{235}U and ^{239}Pu but are spread out more in energy.

DOI: 10.1103/PhysRevC.82.054310 PACS number(s): 23.20.Lv, 25.20.Dc, 27.90.+b

I. INTRODUCTION

Identification and characterization of fissile material is of international concern because of the possibility of proliferation. For safeguard applications, techniques providing isotopic information are necessary [1]. However, few techniques can distinguish between fissile isotopes. Nuclear resonance fluorescence (NRF) is one technique that can be used in applications to identify and quantify isotopic content. It has also been proposed in several detector systems as a viable way to identify fissile material in cargo containers [2,3]. It is necessary to measure the characteristic resonances of all isotopes that are to be distinguished in identification and assay applications.

^{237}Np is of particular interest, as it is fissile [4] yet it is not classified as special nuclear material [5]. The lower regulatory requirements could potentially increase ^{237}Np's attractiveness as a material for diversion in nations with established nuclear programs. ^{237}Np is produced in normal operating conditions in all nuclear reactors that use a uranium fuel cycle. ^{237}Np is formed by the β decay of ^{237}U following two neutron captures on ^{235}U. Its half-life of 2.1×10^6 yr makes it one of the most long-lived components of spent nuclear fuel. In addition, chemical separation techniques exist. A technique that can identify and quantify ^{237}Np is desirable for applications in security and safeguards. Nuclear resonance fluorescence measurements exist for ^{235}U and ^{239}Pu [6,7], and a NRF measurement on ^{237}Np will help complete the data set for fissile isotopes.

Nuclear resonance fluorescence is a process whereby the nucleus is excited to a higher energy state by resonantly absorbing a γ ray. That state then decays by a characteristic γ-ray energy to either the original state or some lower lying excited state, in analog to atomic fluorescence. In the few-electron-volt region around those states that are excited, the excitation cross section is much higher than competing atomic processes. The pattern of electromagnetic resonances forms a unique fingerprint of each nucleus. The high penetrability of γ rays makes them ideal for use in applications where the material in question may be shielded.

This article outlines the NRF measurements on ^{237}Np. The assay of the NpO_2 target used is described. The results are presented in comparison to ^{235}U and ^{239}Pu, and it is shown that the states in ^{237}Np are similar in strength and excitation energy. The results are also compared to systematics for the scissors mode, a mode of nuclear excitation common to heavy, deformed nuclei.

II. EXPERIMENT

Measurements on ^{237}Np were performed using a bremsstrahlung photon source. An electron energy of 2.8 MeV was used. A vertical Van de Graaff electron accelerator housed at the Massachusetts Institute of Technology's High Voltage Research Laboratory produced the electron beam. After the electron beam leaves the accelerator, it is turned 90° by a bending magnet and impinges upon a radiator, producing bremsstrahlung radiation. The radiator consists of a thin gold layer backed by copper. The radiator is electrically isolated

*cangell@nuc.berkeley.edu
†Also at Nuclear Sciences Division, Lawrence Berkeley National Laboratory, Berkeley, California 94720, USA.
‡Present address: Los Alamos National Laboratory, Los Alamos, New Mexico 87545, USA.

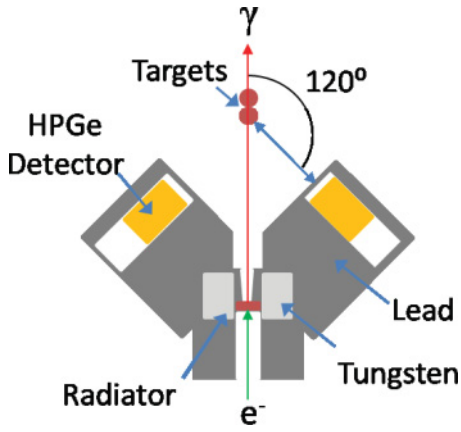

FIG. 1. (Color online) The experimental setup. The small target was placed directly downstream from the large target.

from the surrounding environment, and the beam current incident on the radiator was measured. Average beam currents were recorded on the order of 50 μA. The bremsstrahlung photons are collimated by a Pb block 20 cm long with a 2.5° half-angle conical opening. The experimental setup is shown schematically in Fig. 1.

The target material was aligned to the center of the beam using a Perkin-Elmer x-ray imager downstream of the target. Four high-purity Ge (HPGe) detectors with 100% relative efficiency (to a standard NaI detector) were placed at 120° back-angles from the target. Two detectors were placed on each side, one on top of the other, surrounded by Pb shielding to reduce background. Pb shielding 61 cm thick was placed between the radiator and the detectors to shield the detectors from the intense bremsstrahlung source. An additional 18 cm of tungsten was placed between the radiator and detectors. A 2.5-cm Pb plate was placed in front of the detectors to attenuate low-energy photons coming from atomic scattering of the beam in the target. Detector efficiencies were determined using a ^{56}Co source placed in the target positions. Data were collected using multichannel analyzers. The count rates in the detectors were 400 Hz on average, and the dead time was approximately 5%.

Two targets were used, placed back to back in the beamline. They consisted of NpO_2 powder doubly encapsulated in polyethylene vials. The inner vial had a 1.4-cm inner diameter, while the outer vial had a 2.0-cm inner diameter. The larger sample (9 g NpO_2) was placed upstream of the smaller one (2 g NpO_2) at 80.0 and 83.3 cm from the radiator, respectively. Two tantalum foils weighing 8.8 g in total were used as flux monitor with one wrapped around each sample, minimizing geometric differences. The ratio of foil masses was chosen to correspond to the ratio of target masses. The bremsstrahlung beam diameter was five times (four times) larger than the diameter (height) of the foils. The much greater size of the diameter of the beam, and the distance from the radiator, ensured a uniform flux distribution over the area of the foil and target. A correction was applied to account for attenuation of the beam through the target affecting flux measurements (see Sec. IV). The tantalum foil was sufficiently thin (0.08 mm) to ensure that attenuation through the foil was negligible.

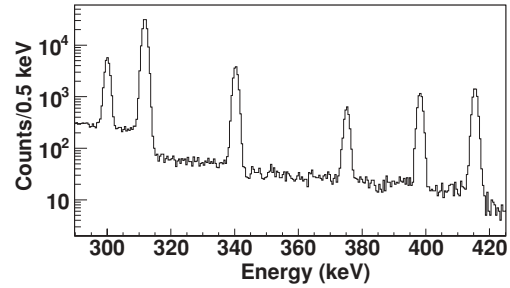

FIG. 2. The six ^{233}Pa lines used to assay the ^{237}Np mass. Spectrum is from 100 sec of live counting, with detector 2 m from target.

III. ^{237}Np ASSAY

The assay of the ^{237}Np targets was performed by placing them, one at a time, 188 cm from a HPGe detector without a Pb attenuator. Six γ-ray lines from the β decay of ^{233}Pa ($t_{1/2} = 27$ d) were used for the assay and ranged in energy from 300 to 400 keV. ^{233}Pa is in secular equilibrium with ^{237}Np ($t_{1/2} = 2.1$ My). Figure 2 shows the spectrum of the ^{233}Pa γ rays emitted from the target assay. A 1.83-μCi ^{152}Eu source was used to determine the detector efficiency in the assay position.

The ^{237}Np mass was determined from the assay for each of the six observed γ-ray lines by using the following formula:

$$m = \frac{N_\gamma}{t\,\epsilon\,I_\gamma\,\overline{f}}\,\frac{\tau_{1/2}}{\ln(2)}\,\frac{M_{\mathrm{Np}}}{N_A}, \tag{1}$$

where N_γ is the number of integrated counts in the peak, t is the time of measurement, ϵ is the detector efficiency for that γ-ray energy, I_γ is the decay intensity, $\overline{f}$ is the average attenuation factor, $\tau_{1/2}$ is the half-life of ^{237}Np, M_{Np} is the molar mass of Np, and N_A is Avogadro's number. The attenuation factors are calculated from the sample density and composition:

$$f = e^{-\mu(m_f)\,\rho\,t}, \tag{2}$$

where $\mu(m_f)$ is the linear attenuation coefficient that depends on m_f, the mass fraction of NpO_2, ρ is the density, t is the target thickness, and m_f is defined as the NpO_2 mass divided by the total target mass. The average attenuation factor, $\overline{f}$, is determined by integrating the attenuation factor over the entire sample area, taking into account the differences in t.

The effect of the presence of a light element in the sample on the γ-ray attenuation factor was investigated by calculating the attenuation factor assuming a variety of light elemental compounds lighter than Cr. The linear attenuation coefficient from the National Institute of Standards and Technology's XCOM database [8] was used. No dependence on the light-element contaminant was found. This indicates that the attenuation is dominated by the photoelectric absorption by Np. The attenuation factor as a function of m_f was also analyzed. The attenuation factors for the six different γ-ray energies all vary linearly with m_f.

An iterative procedure was adopted to accurately obtain the ^{237}Np mass of the target. The target composition (m_f) was not known initially, and density was not known well enough to accurately determine the ^{237}Np mass directly from Eq. (1). The final assay mass was constrained by the self-consistent

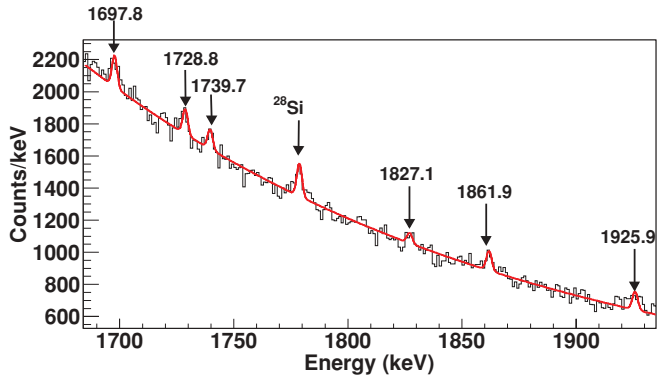

FIG. 3. (Color online) Spectrum observed in ^{237}Np from 1650 to 1950 keV. A line has been drawn to highlight the peaks above background. The energy in kilo-electron-volts is given above the peak. The first excited state in ^{28}Si is visible at 1779 keV, indicating the presence of Si in the sample.

requirement that the mass fraction, m_f, used in determining the attenuation coefficients reproduce the same corresponding ^{237}Np mass. It was further constrained by requiring that the six γ-ray lines all produce the same sample mass. The ^{237}Np mass fraction and target density were varied until these two constraints were satisfied. The final uncertainty was dominated by the input systematic uncertainties. The detector efficiency uncertainty of 4%–6% was the largest contributor to the final uncertainty.

The mass of ^{237}Np was determined to be 7.9 ± 0.5 g in the large sample and 1.78 ± 0.06 g in the small sample. The total ^{237}Np mass is 9.7 ± 0.5 g and the total NpO_2 mass is 11.0 ± 0.6 g. The total target mass is 12.61 g. Both samples were determined to have a contaminant mass fraction of roughly 12% of the sample. The light-element contaminant is 1.6 ± 0.6 g and was determined to be mostly silicon using the several methods described here.

The light-element contaminant was investigated by measuring x rays from the self-fluorescence of the sample. The γ rays and x rays from the decay of ^{237}Np and ^{233}Pa will x-ray fluoresce any material in the sample. The low-energy x rays from the sample were measured using a planar HPGe detector sensitive down to 5-keV x-ray energy. No x-ray lines were observed other than those from the known actinide composition. There are no significant contaminants heavier than Cr in the sample.

The first excited state of ^{28}Si at 1779 keV was fluoresced in the NRF experiment (see Fig. 3). The mass of Si was determined to be 1.2 ± 0.2 g using the measured counts and known half-life of the state. A natural isotopic abundance of Si was assumed. This value is within uncertainty of the mass of the light-element contaminant of the sample determined from the assay. It is also possible that the Si is present as a chemical compound, possibly SiC, as suggested by the jet-black color of the target powder.

The presence of a silicon contaminant in the target was verified by using the scanning transmission x-ray microscope (STXM) end station of the Advanced Light Source–Molecular Environmental Sciences (ALS-MES) beamline. The ALS-MES STXM conducts near-edge x-ray absorption fine structure (NEXAFS) spectromicroscopy from approximately 120 to 2100 eV with a spatial resolution of better than 25 nm [9,10]. This energy range spans the K edges of C, N, O, F, Na, Mg, Al, and Si; the $L_{2,3}$ edges of the first-row transition metals; many of the lanthanide $M_{5,4}$ edges; and the actinide $N_{5,4}$ edges ($4d_{5/2,3/2}$). From these measurements, spectral and elemental information for a single position or a selected area can be extracted.

For the STXM measurement, samples of the NpO_2 particles were prepared in the normal manner [9]. Several particles from both NpO_2 containers were examined between 190 and 1900 eV by collecting NEXAFS spectra and/or elemental maps from which composition information could be determined. Neptunium and oxygen were found at the expected ratios in the particles. The only contaminants found in significant quantities were carbon and silicon. The particles contained evenly distributed silicon consistent with that found in the NRF signal.

IV. ANALYSIS

Runs were taken in four configurations to verify the origin of observed NRF peaks and subtract beam-related background: Np targets with Ta foil (10 h), Np only (13 h), Ta only (6 h), and blank (1 h). A total of fifteen peaks that could be positively identified with ^{237}Np (see Figs. 3 and 4) were observed. They can be used to identify and quantify ^{237}Np in security and safeguards applications, potentially using higher current sources. Each is interpreted as being associated with exciting a single state in ^{237}Np and is observed for the first time. Each peak satisfies the criterion of being observed in both the Np-plus-Ta and Np-only runs, and not seen in the Ta-only or blank runs, and that the peak area is 3σ above background. Additionally, they satisfy the condition that their full width at half maximum (FWHM) is consistent with the calibrated FWHM of the detector determined from ^{56}Co. The observed lowest energy state is at 1698 keV, and the observed highest energy state is at 2506 keV. The strongest observed state was at 1729 keV (see Table I).

A triplet of states was observed at 2378 keV (see Fig. 5). Their combined strength is comparable to that of the strongest state at 1729 keV. They are useful in an applications setting

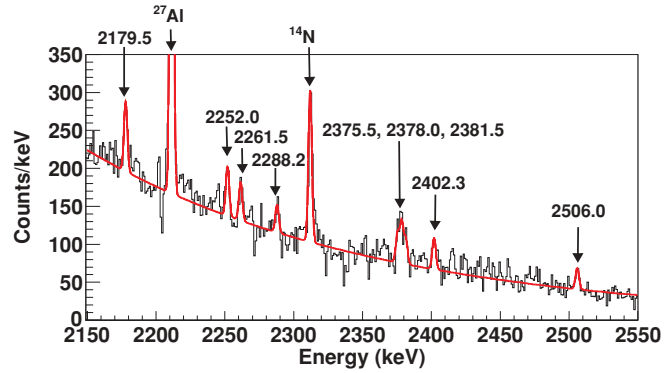

FIG. 4. (Color online) Same as Fig. 3, except now between 2150 and 2550 keV. Background peaks from ^{27}Al (from the detector stand) and ^{14}N (from air) are visible.

TABLE I. ^{237}Np NRF-integrated cross sections.

Energy (keV)	I_{cs} (eV barn)
1697.8 ± 0.5	5.3 ± 1.4
1728.8 ± 0.2	10.6 ± 2.3
1739.7 ± 0.4	4.8 ± 1.4
1827.1 ± 0.6	5.7 ± 1.4
1861.9 ± 0.3	5.6 ± 1.5
1925.9 ± 0.8	6.1 ± 1.5
2179.5 ± 0.7	7.2 ± 1.8
2252.0 ± 0.3	7.3 ± 1.6
2261.5 ± 0.5	7.8 ± 1.9
2288.2 ± 0.3	4.6 ± 1.1
2375.5 ± 0.3	4.9 ± 1.2
2378.0 ± 0.3	2.7 ± 0.7
2381.5 ± 0.3	2.7 ± 0.7
2402.3 ± 0.4	4.4 ± 1.1
2506.0 ± 0.7	3.8 ± 1.0

for increasing detection probability in the case where lower-resolution detectors are used.

In addition to the peaks from ^{237}Np, three peaks were identified that are from the fluorescence of other isotopes. At 1779 keV, a peak that comes from the first excited state in ^{28}Si (see Fig. 3) is seen. This is from the Si contaminant in the sample. At 2212 keV, a peak is seen from ^{27}Al (see Fig. 4). The detectors were placed on a large Al table, and it is suspected that the ^{27}Al was being excited by the beam halo. At 2312 keV, a peak is seen corresponding to the first excited state of the ^{14}N in the air being fluoresced.

The integrated cross section can be determined from the observed peak area and is given by

$$I_{cs} = \frac{N_p}{N_t \, \epsilon \, \Phi \, \overline{f_t} \, x_{LT}}, \tag{3}$$

where N_p is the number of counts in the peak, N_t is the number of ^{237}Np atoms in the sample, ϵ is the detector efficiency, and x_{LT} is the live time. The variable $\overline{f_t}$ is the average attenuation factor, as a function of γ-ray energy, for the γ rays entering and leaving the target as first the beam, then the fluoresced γ rays. It was obtained by averaging over the entire target volume.

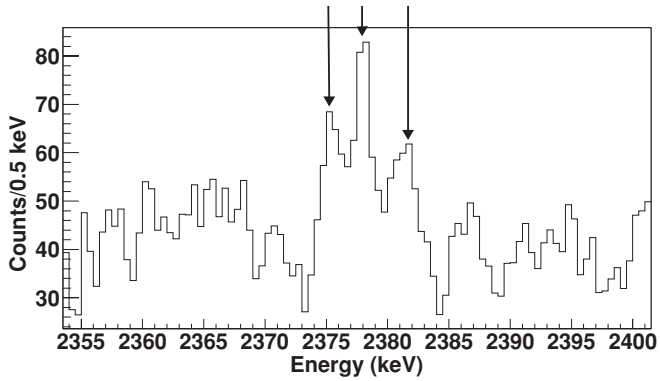

FIG. 5. The peak triplet observed around 2378 keV. This triplet has a combined strength of about 10 eV barn, comparable to the strongest single state observed. They are useful in an applications setting for increasing detection probability in the case where lower resolution detectors are used.

The flux, Φ, is energy dependent, and was obtained by normalizing the Schiff formula for bremsstrahlung production [11] to a known line in ^{181}Ta. The 2297-keV state in ^{181}Ta was used and has an integrated cross section of 23.6 eV barn [12]. A small correction for attenuation of γ rays through the target was applied to the flux. The attenuation was calculated by integrating over the cylindrical cross section for γ rays fluorescing the Ta foil behind the target or for scattered γ rays that must then travel back through the target to the detector and weighting it by the amount of foil being obstructed. Accounting for the attenuation introduced a correction to the flux of 1%.

The peaks and obtained integrated cross sections are given in Table I. The final uncertainties includes both statistical and systematic uncertainties added in quadrature. They are dominated by the statistical uncertainties in the integrated peak counts. The systematic uncertainties includes the flux normalization to the ^{181}Ta peak (10% uncertainty) and the target mass (5% uncertainty).

V. COMPARISON AND DISCUSSION

This NRF measurement on ^{237}Np completes the set of three odd-mass actinides that includes ^{235}U and ^{239}Pu (see Fig. 6). Comparing the three nuclei shows how the position and strength of the observed states transform as a proton-neutron pair is added in each step. The states observed have a mean excitation energy of 1.8 MeV in ^{235}U and around 2.3 MeV in ^{239}Pu, giving an energy separation of 500 keV. The states in ^{237}Np are roughly split into two groups. The mean excitation energy of one group roughly corresponds with the mean excitation energy of ^{235}U, and the energy of the other group corresponds with that of ^{239}Pu. As the mass of the system increases, the mean excitation energy goes to higher energy. The average integrated cross section of states is similar in all three nuclei. The observed states are likely all from a common excitation mode.

The splitting in ^{237}Np may arise from the coupling of the excited mode to the odd-proton single-particle states, which is similarly seen in other odd-even nuclei [12]. The mixing with single-particle excitations is expected to be stronger in odd-proton nuclei compared to odd-neutron nuclei [13]. The coupling of the odd nucleon to the even-even core distributes the strength to many levels becuase of the several ways the nucleon can couple to each of the states present in the nucleus.

The observed states may be part of the scissors mode. The scissors mode is an $M1$ orbital mode of excitation in deformed nuclei. It is characterized by the neutron and proton oscillating against each other out of the plane of rotation, in a "scissors"-like manner. The scissors mode has been observed in nearly all heavy, deformed nuclei [13]. Whether or not the observed states are part of the scissors mode can be examined by comparing them with expectations from theory. The $\sum B(M1)\uparrow$ (single-particle) strength of the scissors mode can be calculated from a sum rule [14]. The sum rule requires two inputs: the mean excitation energy and the

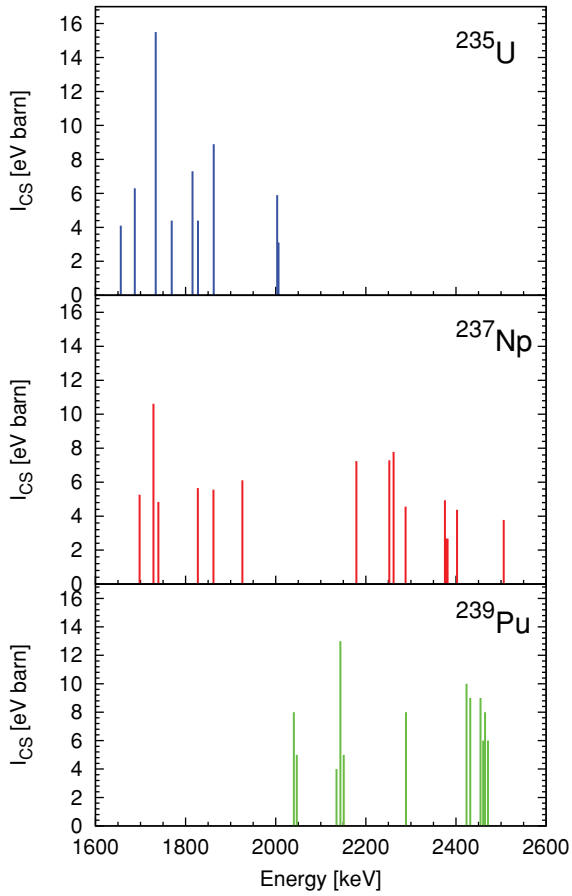

FIG. 6. (Color online) The integrated cross section (I_{cs}) for ^{235}U [6,7], ^{237}Np (present results), and ^{239}Pu [6]. The results from ^{237}Np show how the mean excitation energy and splitting of the states transforms with an increase in mass. The values for ^{235}U use the results of Yevetska *et al.* [7] and Bertozzi *et al.* [6] averaged together, except for the states at 1.66 and 1.77 MeV, which were only observed by Bertozzi *et al.*

ground-state deformation. The mean excitation energy was taken from the experimental results, and a deformation of $\delta = 2.45$ was taken from the RIPL-2 compilation [15]. The $B(M1)\uparrow$ value for each state can be calculated from the integrated cross section, assuming that the transition is $M1$ in nature. The $\sum B(M1)\uparrow$ strength is obtained by adding together the individual strengths.

The experimental $\sum B(M1)\uparrow$ strength is $0.92 \pm .06\mu_n^2$, and the sum rule value is 2.71 μ_n^2. If the scissors mode has been observed, then about three times more strength is to be expected. If only some of these states are $M1$ transitions, then even more strength is expected. Odd-mass nuclei have long been characterized as having an apparent deficit of scissors-mode strength [12]. This deficit has been attributed to a fragmentation of the strength, resulting in many states that are below the experimental limit of detectability. More sensitive experiments can test this hypothesis.

VI. CONCLUSION

In conclusion, we observed fifteen new states in ^{237}Np in the first NRF measurement on ^{237}Np. The measurements were done using a bremsstrahlung source of γ rays. States were observed over the range of 1.7–2.5 MeV. These states can be used to identify and quantify ^{237}Np in applications for security and safeguards.

The Np targets were assayed by measuring the γ rays from the decay of target nuclei and the x rays from the self-fluorescence of the target, and by STXM measurements done at the ALS-MES. It was confirmed in all three techniques that the target was mostly NpO_2, with a light-element contaminant that was identified as Si in the NRF and STXM measurements.

The observed states' integrated cross sections are similar to those found in ^{235}U and ^{239}Pu [6,7] and may be from the same excitation mode. They are split into two groups. The mean excitation energy of one group roughly corresponds with the mean excitation energy of ^{235}U, and the energy of the other group corresponds with that of ^{239}Pu. This is interpreted as the coupling of the odd proton in ^{237}Np increasing the energy splitting of the observed excitation mode. The mean energy of the excitation mode is also interpreted as increasing with increasing mass. The observed states may be a part of the scissors mode of excitation, in which case roughly three times more strength would be expected.

ACKNOWLEDGMENTS

This research was funded by the US Department of Homeland Security. Parts of this research and the ALS were supported by the Director, Office of Science, Office of Basic Energy Sciences and the Division of Chemical Sciences, Geosciences, and Biosciences of the US Department of Energy at Lawrence Berkeley National Laboratory under Contract No. DE-AC02-05CH11231.

[1] S. J. Tobin *et al.*, in *Institute of Nuclear Materials Management 50th Annual Meeting*, Tucson, AZ, 2009 (LA-UR 09-03748).
[2] W. Bertozzi, S. E. Korbly, R. J. Ledoux, and W. Park, Nucl. Instrum. Methods B **261**, 331 (2007).
[3] J. Pruet, D. P. McNabb, C. A. Hagmann, F. V. Hartemann, and C. P. J. Barty, J. Appl. Phys. **99**, 123102 (2006).
[4] R. Sanchez, D. Loaiza, and R. Kimpland, Trans. Am. Nucl. Soc. **88**, 88 (2003).
[5] "Nuclear Regulatory Legislation: 110th Congress," Tech. Rep. NUREG-0980 (Nuclear Regulatory Commission, 2009).
[6] W. Bertozzi, J. A. Caggiano, W. K. Hensley, M. S. Johnson, S. E. Korbly, R. J. Ledoux, D. P. McNabb, E. B. Norman, W. H. Park, and G. A. Warren, Phys. Rev. C **78**, 041601 (2008).
[7] O. Yevetska, J. Enders, M. Fritzsche, P. von Neumann-Cosel, S. Oberstedt, A. Richter, C. Romig, D. Savran, and K. Sonnabend, Phys. Rev. C **81**, 044309 (2010).
[8] M. Berger, J. Hubbell, S. Seltzer, J. Chang, J. Coursey, R. Sukumar, and D. Zucker, "Xcom: Photon cross sections database," (1998) [http://www.nist.gov/physlab/data/xcom/index.cfm.].

[9] D. Shuh, in *Speciation Techniques and Facilities for Radioactive Materials at Synchrotron Light Sources*, NEA 6288 (OECD, Karlsruhe, Germany, 2007), pp. 125–134.
[10] H. Bluhm *et al.*, J. Electron Spectrosc. Relat. Phenom. **150**, 86 (2006).
[11] L. I. Schiff, Phys. Rev. **83**, 252 (1951).
[12] A. Wolpert *et al.*, Phys. Rev. C **58**, 765 (1998).
[13] U. Kneissl, H. Pitz, and A. Zilges, Prog. Part. Nucl. Phys. **37**, 349 (1996).
[14] N. L. Iudice and A. Richter, Phys. Lett. B **304**, 193 (1993).
[15] T. Belgya *et al.*, *Handbook for Calculations of Nuclear Reaction Data, RIPL-2*, Tech. Rep. IAEA-TECDOC-1506 (IAEA, Vienna, Austria, 2006).